The upper end of the observed cosmic ray energy spectrum

1974 J. Phys. A: Math. Nucl. Gen. 7 990

(http://iopscience.iop.org/0301-0015/7/8/007)

J. Phys. A: Math., Nucl. Gen., Vol. 7, No. 8, 1974. Printed in Great Britain.

The upper end of the observed cosmic ray energy spectrum

C J Bell, A D Bray, S A David, B V Denehy, L Goorevich, L Horton, J G Loy, C B A McCusker, P Nielsen†, A K Outhred, L S Peak, J Ulrichs, L S Wilson and M M Winn

Cornell–Sydney University Astronomy Centre, University of Sydney, Sydney, NSW 2006, Australia

Received 30 October 1973, in final form 10 December 1973

Abstract. The Sydney giant air shower array has been in operation now for approximately five years. This paper analyses the first 10 000 showers observed and derives a muon size and total energy spectrum. The area time product involved for these data is about 175 km^2 yr and the threshold energy for these showers is about 10^{17} eV.

The detection probability of the array is carefully analysed by simulated showers and associated errors are assessed.

The resulting energy spectrum is derived using a variety of shower development models from both Sydney and Haverah Park. Latest Monte Carlo and analytical air shower calculations provide the necessary link between the observed number of muons and the primary energy.

The Sydney energy spectrum is compared with those from Moscow, Volcano Ranch, Mount Chacaltaya and Haverah Park.

No significant change in slope is seen from 10^{17} eV to about 10^{20} eV and the data are best summarized by the spectrum

$$J(>E) = 10^{-12\cdot03\pm0\cdot01}\left(\frac{E}{10^{18}\,\mathrm{eV}}\right)^{-1\cdot96\pm0\cdot02} \mathrm{m^{-2}s^{-1}sr^{-1}}$$

for energies in the range $10^{17\cdot25} \leqslant E \leqslant 10^{20\cdot25}$ eV.

1. Introduction

The Sydney University giant air shower recorder has been in operation since January 1968, and had recorded 10 065 showers up to October 1972. This paper is concerned with the primary energy spectrum derived from these showers. The total detection area–time product for the array over this period is 175 km^2 yr, compared with (at October 1972) Haverah Park 45 (of which only 15 km^2 yr are used in the determination of their energy spectrum given in Edge *et al* 1973) Yakutsk 33, Volcano Ranch 30, Tokyo 6 and Cornell 2 km^2 yr (approximately).

2. The Sydney University giant airshower recorder (SUGAR)

2.1. The SUGAR array

The SUGAR array is located in the Pilliga State Forest, New South Wales, at latitude 30° 31′ S, longitude 149° 38′ E and altitude 250 m. It consists at present (July 1973) of

† Now with the Australian National Antarctic Research Expeditions.

47 independent stations on a rectangular grid, side directions north–south and east–west, with grid sizes 200 m, 400 m, 800 m and 1600 m (approximately). The layout is shown in figure 1.

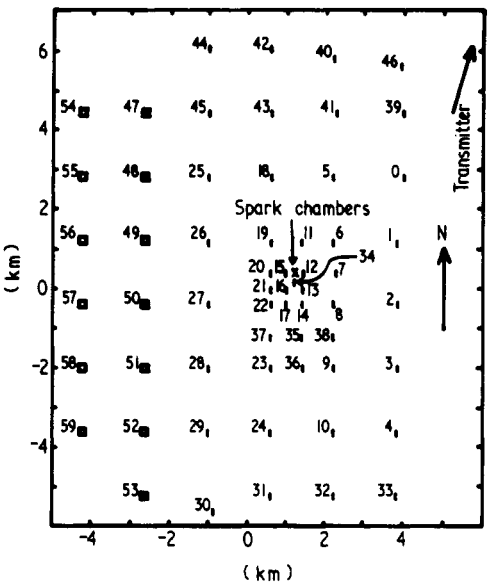

Figure 1. A map of the SUGAR Pilliga array. ■ Stations operating March 1973, □ stations not yet installed.

2.2 The SUGAR station

Each SUGAR station consists of two tanks of liquid scintillator buried in the ground 50 m apart. Each tank is shaped like an inverted funnel with the photomultiplier at the centre looking down. The scintillator is at the base of the funnel, an area of 6 m^2. The floor of the tank is in the shape of a shallow cone, designed to present to the photomultiplier tube the same light intensity for particles traversing the scintillator at different distances from the axis of the funnel. The depth of earth shielding the scintillator is $1{\cdot}5 \pm 0{\cdot}3$ m.

The scintillation from a single, vertical, minimum-ionizing muon traversing the tank produces an average of 10 photo-electrons from the cathode of the 7 in EMI 9623b photomultiplier. Electron multiplication within the photomultiplier is of the order of 5×10^6, and the charge is deposited on a 140 pF capacitance. Voltage amplification by a factor of 1250 then occurs, and the resulting pulse is compared with a discrimination level corresponding to the passage of three vertical muons through the tank.

If both tanks of a given station record pulses exceeding the discrimination level and within 350 ns of each other, a coincidence or local event occurs. In this case the recording apparatus of the station is switched on, and the time of the event, the height of the pulse from each tank ('channel') and the difference in time between the tanks is recorded.

A decay resistor on the capacitor which stores the photomultiplier charge produces a logarithmic pulse height-to-time conversion with a time constant of 3 μs. The length of the resulting pulse is digitized at 10 MHz, so that one count corresponds to a 3·4% change in pulse height.

The time of a local event is determined relative to a timing pattern transmitted from a central clock (whose position is indicated in figure 1), to an accuracy of ± 50 ns; this is achieved by means of a local vernier oscillator. (The timing will be described in more detail in a subsequent paper on the arrival directions of high energy cosmic rays.)

Local event information is recorded serially in triplicate on $\frac{1}{4}$ in acoustic magnetic tape. The tape at each station is changed every 7 to 10 days, and the full tapes are sent to Sydney for analysis.

3. SUGAR data analysis

The SUGAR array produces a set of independent station records of local events. The processing of these records involves their transfer to computer files, and the decoding and calibration. Array events (coincidences between three or more stations) are found and analysed for the direction of origin of the incident shower and its muon size and core position. The muon size and zenith angle determine, via a shower model, a cosmic ray primary energy, which in conjunction with estimates of the effective-detecting-area–time product yields a primary energy spectrum.

The determination of the muon size of a shower requires knowledge of the muon lateral structure function, which has been studied in a maximum likelihood process applied to the observed events. Assignment of a primary energy requires theoretical estimates of the development of a shower through the atmosphere; restrictions have been placed on such models by observation of the 'development' of the muon showers with zenith angle. The effective area of the array at any time is calculated from the operating records of the individual stations.

3.1. Decoding and calibration

The records of local events for each station are transferred to computer tape and at the same time are checked for conformity to the correct format. As indicated, each event is recorded in triplicate. Any event for which two or three copies conform to the format and agree with each other, is accepted. The data are then decoded, and again checked for time sequence and for conformity with expected count ranges in the vernier timing. A manual check is also made on the pulse-height spectrum of a set of local events, and on other features. When an event is rejected, for any reason, the station is said to be inoperative from just after the last accepted event until just before the next one. A 'dead' time of 10 seconds is also allowed after each local event; for the remainder of the time, the station is 'live'.

Accepted events then have their pulse-length count for each tank converted into an equivalent number of vertical muons' using calibration data obtained from artificially initiated (simulated) local events which occur regularly at each station. The simulated events monitor the calibration of four pulse heights across the range of the apparatus, and two points on the single-tank integral pulse-height spectrum.

3.2. Array events

An array event consists of coincident local events from three or more stations, the coincidence interval being 80·5 μs (2^{-30} days, which is one period of the central timing clock). Array events for which the coincident stations are collinear or for which the

recorded times of arrival of the shower front at each station yield an unphysical arrival direction (fluctuations from steeply inclined showers) are rejected from further analysis. Otherwise, a least-squares plane shower front is fitted to the station times to give a first estimate of the arrival direction. More sophisticated direction analysis is carried out later, but is not the subject of this paper.

Using this first estimate of the arrival direction, a core position and muon size are fitted to the responses by a maximum likelihood process. The muon size, here, is the number of muons whose energy exceeds the threshold for detection by a SUGAR tank, namely $(0{\cdot}75 \pm 0{\cdot}15) \sec\theta$ GeV where θ is the zenith angle of the shower.

In fitting the core position and shower size, account is taken both of those stations which did record local events, and those which did not. The likelihood of a given muon size N_μ is also weighted according to the *a priori* probability of that N_μ, which is proportional to the differential spectral intensity $N_\mu^{-\gamma}$. (An approximate value, $\gamma = 3$, is used.)

The core search uses two grid sizes determined by the total number of particles detected, and is repeated. The first search starts at a point 'interior' to the three largest station responses, and the second 'exterior'.

The muon lateral distribution, or structure function, used is that determined by Fisher (1970) and reported in Brownlee *et al* (1970). It is a modified version of the Greisen muon structure function (Bennett and Greisen 1961) with the exponent of the distant term being zenith dependent:

$$\rho(\mu) = N_\mu k(\theta) r^{-0{\cdot}75}\left(1+\frac{r}{320}\right)^{-(1{\cdot}50+1{\cdot}86\cos\theta)}$$

where $k(\theta)$ is a normalization constant. This function is shown for several zenith angles in figure 2.

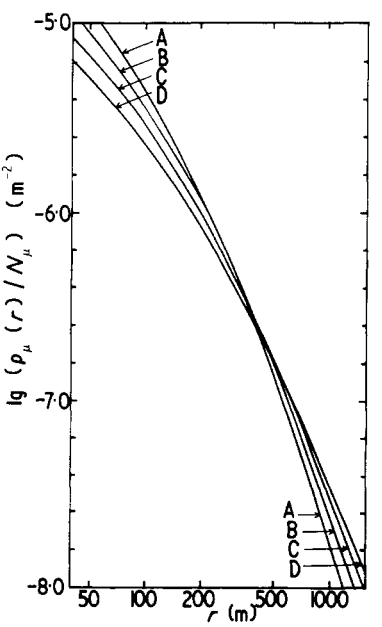

Figure 2. The SUGAR muon structure function, for four values of the zenith angle θ. Curve A, $\theta = 0°$; curve B, $\theta = 45°$; curve C, $\theta = 60°$; curve D, $\theta = 75°$.

This function was derived from a study of showers of muon size between 10^6 and 10^7 particles. The largest showers, which determine the upper end of the spectrum have sizes between 10^8 and 10^9. Figure 3 shows the observed densities of 13 large showers with sizes from 1·3 to $9{\cdot}5 \times 10^8$ muons ano zenith angles less than 45°. The densities are normalized to a size of $N_\mu = 4{\cdot}5 \times 10^8$ and compared with the Fisher structure function for a shower of that size and zenith angle 35°. Up to 1000 m from the core *all* stations in these showers gave non-zero readings so well determined densities can be given. Beyond that distance, in some showers, some stations in a given annulus were not triggered. In that case two readings are given. If μ is the total number of muons recorded by the stations and if n tanks out of a possible N gave non-zero readings then the lower limit for the density is μ/NA where A is the area of one tank. An estimate of an upper limit is μ/nA. Of the 45 well determined density readings 36 lie within one standard deviation of the Fisher curve if we allow a core error of ± 50 m. The one apparently high point at 220 m is due to the effect of very high particle densities on our scintillators. Normally we do not use densities greater than 700 particles m^{-2}. We conclude that the structure function is independent of shower size in the range $10^6 \leqslant N_\mu < 10^9$.

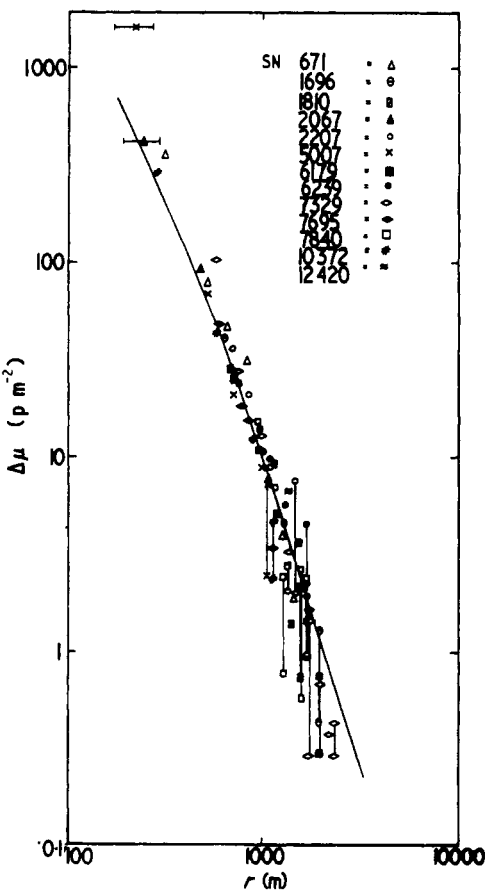

Figure 3. The muon lateral distribution function for 13 large showers with $10^8 < N_\mu < 10^9$ particles and $\theta < 45°$. The densities are normalized to a shower size of $4{\cdot}5 \times 10^8$. The curve is the Fisher structure function for that size and $\theta = 35°$.

3.3. A Monte Carlo test for errors and analytical bias

To test the reliability of the analysis, a set of showers has been simulated in the computer by a Monte Carlo method. The primary energy of each shower was assigned from a spectrum

$$J(E)\,dE = 5\times 10^{23}E^{-3\cdot0}\,dE\,m^{-2}\,s^{-1}\,sr^{-1} \qquad (E \text{ in eV}).$$

The zenith angle was assigned from an appropriate distribution, and the azimuth angle and core position at random. Using a standard E–N_μ theoretical conversion a muon size was assigned to each shower. The experimental SUGAR structure function then predicted the responses at the individual stations. Fluctuations in muon size for a given primary energy and zenith angle, and in observed muon density and detection time at each station were incorporated. The status of each station was assigned according to typical station records.

The responses generated in this way were then subjected to the normal analysis. The parameters fitted by this analysis (zenith angle, core position, muon size, primary energy) were then compared with those generated by the Monte Carlo process. Figure 4

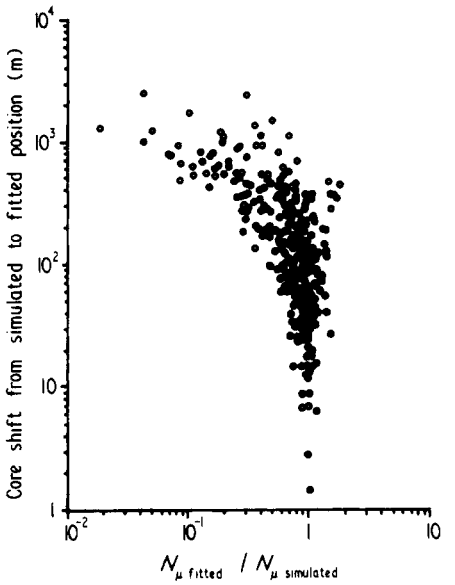

Figure 4. The relationship between the shift in core position and the change in muon size, from the values simulated to those fitted by the standard SUGAR analysis.

compares the shift in core position with the change in muon size. It can be seen that considerable changes in core position occurred; however, the greatest changes were associated with reductions in muon size rather than increases, and since the spectrum slopes steeply downwards, their effect on it will be slight. The net reduction lg N_μ in the analysis was:

$$\lg\left(\frac{N_\mu(\text{fitted})}{N_\mu(\text{simulated})}\right) = -0{\cdot}16.$$

The corresponding figure for the primary energy E_p was $-0{\cdot}15$. The standard deviation

of $\lg[E_p(\text{fitted})/E_p(\text{simulated})]$ was somewhat dependent on E_p, ranging from 0·40 to 0·23 as the energy increased. There was no net change in zenith angle θ, and the standard deviation of $\theta(\text{fitted}) - \theta(\text{simulated})$ was 2·6°.

3.4. Errors from events of small multiplicity

Most of the large showers were picked up by the large array, which over most of its area has a spacing of 1·6 km between stations. Thirty-two of these events involved only three stations (it is worth remembering that this means six scintillators). If these small multiplicity events had large errors in their primary energies, particularly if these errors were overestimates, then the spectrum would be badly distorted.

Fortunately it is possible to determine the errors experimentally. In the same sample of showers with $\theta < 60°$ and at least three stations of the 1·6 km array involved, twenty-two had seven or more stations involved. These were events that fell sufficiently close to the central part of the array to involve stations on the 0·8 and 0·4 km grids. The mean number of stations in these events was 9·2 (ie 18·4 scintillators). Because of this, all parameters were very well determined.

To find the errors for small multiplicity events we have recalculated the parameters for these showers, turning off all stations except those on the 1·6 km array. When this is done the mean multiplicity of the twenty-seven events is 3·3. We find that the new primary energy is, on average, only 10% *lower* than the original estimate. The largest overestimate of the new energies was only a factor of 1·36. In 70% of the cases the shift in the energy would not move it out of the energy bin in which it was originally placed.

4. Array effective detecting area

The effective detecting area of the array at any particular time, A_{eff}, can be expressed in terms of the probability p that a shower falling within the physical area A will be detected:

$$A_{\text{eff}} = Ap.$$

For the SUGAR array, p is calculated by a Monte Carlo method. Showers of a given muon size and zenith angle, with random azimuth and core position, are simulated over the array, and the average probability of detection calculated. The density of the showers is varied to suit the station grid size in different parts of the array. The contribution of each shower to the average probability is weighted according to the region. A boundary region extending beyond the physical boundary of the array is included to allow for showers (especially at high zenith) falling outside the array and being relocated within. (Such showers are often not greatly reduced in size†.)

The probability that any given shower will be detected takes account of the operating record of each station, using the proportion of the total time under consideration for which that station was 'live'. This assumes that the inoperative periods of different stations are uncorrelated. In fact, systematic extensions and modifications to the array have occurred, so that the total operating time of the array has been divided into periods T_i such that the assumption is true, for each period. The effective detecting area for each

† The energy spectrum has also been calculated using boundaries on and within the physical boundary of the array, and aside from the exclusion of three of the largest showers (two of which had cores actually placed *on* saturated scintillator tanks on the array boundary) there was no significant change in the shape of the spectrum.

period, $Ap_i(N_\mu, \theta)$, is calculated, and the total effective-area–operating-time product is given by

$$(AT)_{\text{eff}} = \sum_i AT_i p_i(N_\mu, \theta).$$

The muon structure function used for the simulated showers is the same as that used in the standard shower analysis (see § 3.2). To investigate the error involved due to the assumption of a particular structure function, the exponent describing the structure function at large distances was varied from $-2{\cdot}3$ to $-3{\cdot}6$ for showers of various sizes. For $N_\mu \sim 2 \times 10^7$, the resulting change in the detection probability for vertical showers was a factor of about 2.

By way of comparison, the detection probability varies by a factor of about five when the zenith angle changes from 0° to 60° (using the standard SUGAR structure function and a similar shower size).

The error in the effective detecting area calculation arising from the Monte Carlo method used has been estimated by repeating the calculation. The standard deviation of the detection probability resulting from ten calculations, expressed as a percentage of the probability, is shown as a function of muon size in figure 5. The errors have been averaged over zenith angle.

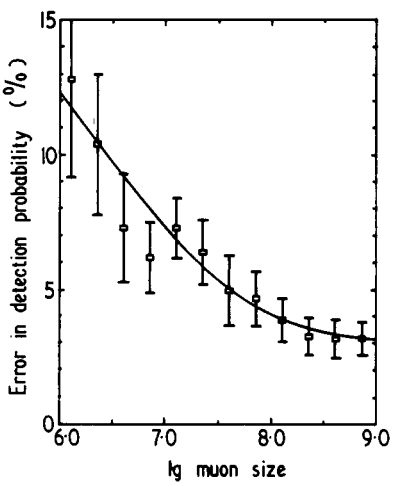

Figure 5. The percentage error in the detection probability calculated for a single period, as a function of muon size.

This, however, is an error relating to a single time interval and the contribution of these errors to spectral intensities is reduced by a factor of about three when the calculation is repeated for all the (25) periods T_i contributing to the total operating time under consideration.

The detection probability calculation has been verified by repeating the calculation using the (completely independent) shower simulation system described in § 3.3. Out of fifteen calculations covering muon sizes 10^7, 10^8 and 10^9, zenith angles 0° and 60° and three array operating periods, thirteen agreed with the standard calculation within one standard deviation.

5. Muon size spectrum

Integral muon size spectra of the form

$$J_N(>N_\mu, \theta) = k_N(\theta) N_\mu^{-\gamma_N(\theta)}$$

have been fitted by a maximum likelihood method to the observed showers grouped into ten zenith angle ranges. The boundaries of the ranges are at

$$\sin^2\theta = 0{\cdot}0, 0{\cdot}1, 0{\cdot}2, \ldots, 0{\cdot}9, 0{\cdot}933.$$

The maximum likelihood estimates of $k_N(\theta)$ and $\gamma_N(\theta)$ for a set of showers $i = 1, \ldots, \nu$ in the zenith range (θ_1, θ_2) and muon size range (N_1, N_2) are given by

$$\langle k'_N(\theta)\rangle = \frac{\nu}{\int_{N_1}^{N_2} N^{-\langle\gamma_N(\theta)\rangle} D_{AT\theta}(N)\,\mathrm{d}N}$$

and

$$\langle k'_N(\theta)\rangle \int_{\ln(N_1)}^{\ln(N_2)} \mathrm{e}^{-\langle\gamma_N(\theta)\rangle \ln(N)} D'_{AT\theta}[\ln(N)]\,\mathrm{d}[\ln(N)] = \sum_{i=1}^{\nu} \ln(N_i)$$

where

$$k'_N(\theta) = \gamma_N(\theta) k_N(\theta)$$

$$D_{AT\theta}(N) = D'_{AT\theta}\ln(N) = \int_{\theta_1}^{\theta_2} AT\,p_{AT}(N, \theta) 2\pi \sin\theta\cos\theta\,\mathrm{d}\theta$$

$$AT\,p_{AT}(N, \theta) = (AT)_{\mathrm{eff}} = \sum_j AT_j p_j(N_\mu, \theta),$$

the projected area of the array in the shower plane is $A\cos\theta$, and the acceptance solid angle $\mathrm{d}\Omega = 2\pi\sin\theta\,\mathrm{d}\theta$.

The results are plotted in figure 6, where pairs of adjacent zenith angle ranges have been combined for clarity. Also shown are the intensities at intervals of 0·25 in $\lg N_\mu$ for each zenith angle. The error bars shown take account of poissonian fluctuations and of the errors in the effective detecting area estimates. The total number of showers recorded within the overall recording time used was 10 065; the number of showers falling within the range used for fitting the maximum likelihood spectra ($6{\cdot}5 \leqslant \lg N_\mu \leqslant 8{\cdot}5$) was 4699.

6. Shower development

The integral muon size spectra allow observation of the 'development' of muon showers with zenith angle. Assuming that there is no zenith dependence of the primary energy spectrum, the same integral intensity at different zenith angles corresponds to the same primary energy. Hence constant intensity cuts across the integral muon size spectra for a set of zenith angle ranges correspond to constant primary energy, or in other words, represent the 'development' of a shower with zenith angle.

6.1. Observed 'development'

Constant intensity cuts across the SUGAR integral muon size spectra described in § 5 are shown in figure 7, with the actual muon sizes interpolated from the spectra shown for

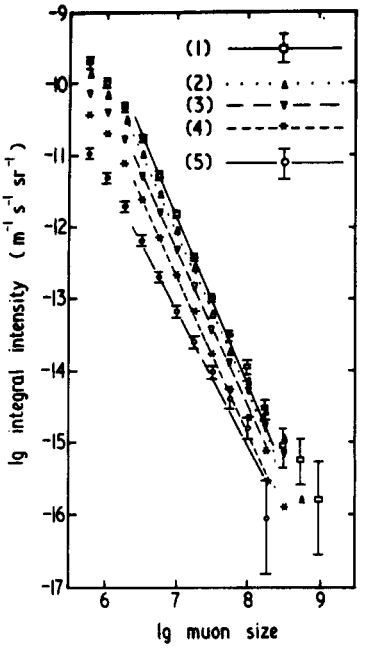

Figure 6. Integral muon size spectra for five zenith angle ranges: (1) $0{\cdot}0 < \sin^2\theta < 0{\cdot}2$, (2) $0{\cdot}2 < \sin^2\theta < 0{\cdot}4$, (3) $0{\cdot}4 < \sin^2\theta < 0{\cdot}6$, (4) $0{\cdot}6 < \sin^2\theta < 0{\cdot}8$ and (5) $0{\cdot}8 < \sin^2\theta < 0{\cdot}933$. The lines are the fitted spectra and the points intensities at intervals of 0·25 in lg N_μ. Error bars are only drawn for ranges (1) and (5).

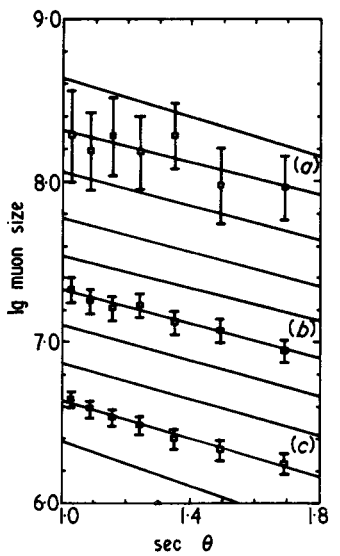

Figure 7. 'Development' curves derived from the integral muon size spectra by interpolation; the lines are weighted least-squares fits to the interpolated muon sizes at intervals of 0·5 in lg integral intensity. The actual interpolated sizes are shown for three intensities (*a*) $10^{-14\cdot5}$ $m^{-2}\,s^{-1}\,sr^{-1}$, (*b*) $10^{-12\cdot5}$ $m^{-2}\,s^{-1}\,sr^{-1}$, (*c*) $10^{-11\cdot0}$ $m^{-2}\,s^{-1}\,sr^{-1}$.

three intensities. The lines are weighted least-square fits to the points. The separation between lines corresponds to a change of 0·5 in lg(integral intensity). These muon sizes are, of course, for muons above the SUGAR threshold of $(0{\cdot}75 \pm 0{\cdot}15) \sec\theta$ GeV. Any theoretical comparison (cf § 6.2) needs to use a similar value.

It is apparent that all the muon showers observed by SUGAR are past maximum development, while tending to become younger with increasing size as expected. The curve for the largest showers is anomalous, but has very low statistical weight, involving numbers of showers in each zenith range of order 1.

The lines of figure 7 represent relationships of the form $N_\mu = N_{\mu 0}\, e^{-\sec\theta/\lambda}$; where λ is the muon shower attenuation length in atmospheres. The atmospheric depth at the array is 1000 g cm^{-2}. λ is shown as a function of $N_{\mu 0}$ in figure 8; a weighted least-squares

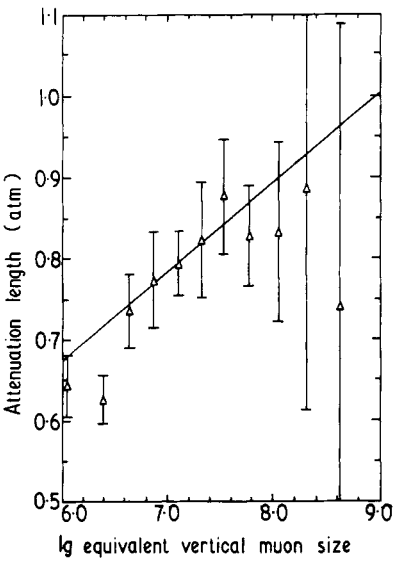

Figure 8. The attenuation length implied by the lines of figure 7, shown as a function of the intercept of each line at $\theta = 0°$.

line has been fitted to the points, excluding the two at smallest shower size; and is represented by

$$\lambda = (0{\cdot}79 \pm 0{\cdot}05) + (0{\cdot}114 \pm 0{\cdot}068) \ln\left(\frac{N_{\mu 0}}{10^7}\right).$$

The two excluded points were derived from data covering only part (near to vertical) of the zenith range used for the remaining points. Since the points in figure 7 are not perfectly fitted by a straight line but rather tend to follow a concave upward shape, the restriction of data to near-vertical tends to produce steeper fitted lines.

The fitted relationship for λ tends to overestimate its size dependence, since once again the points are not really linear but follow a concave downward shape; and further, the points at smaller size, having higher statistical weight, tend to bias the fit towards a stronger size dependence. On the other hand, the relationship quoted at the Denver Conference (Bell *et al* 1973), in which the statistical weighting was removed, probably represents an underestimate of the size dependence of λ.

The development curves have also been represented by relationships of the form $N_\mu = N'_{\mu 0}(\sec\theta)^{-\beta}$, which yields

$$\beta = (1{\cdot}71 \pm 0{\cdot}08) - (0{\cdot}116 \pm 0{\cdot}052)\ln\left(\frac{N'_{\mu 0}}{10^7}\right).$$

The comments on the relationship for λ apply equally to this relationship.

Either of the above forms can be used to assign an equivalent vertical muon size ($N_{\mu 0}$ or $N'_{\mu 0}$) to any given shower (N_μ, θ).

6.2. Comparison with theoretical predictions of 'development'

In order to relate observed air shower parameters to the properties of the primary cosmic ray particles, and in particular muon size to primary energy at a given zenith angle, models of air shower development have been constructed. For the SUGAR experiment, two approaches, one principally Monte Carlo and the other analytical involving the appropriate diffusion equations, have been used. The models are described in McCusker *et al* (1970), Goorevich (1971) and Goorevich and Peak (1973).

Of the Monte Carlo type calculations two sets using an isobar–fireball model with an $E^{1/4}$ secondary multiplicity law, for primary mass numbers 1 and 64 respectively (proton and copper) have been favoured.

The more recent analytical approach has been used in a multiple saturating fireball model, applying to both N–N and π–N collisions. The secondary multiplicity varies asymptotically as $E^{0{\cdot}3}$. One free parameter, χ, specifies the proportion of $N\bar{N}$ decays from the pion resonances in the π–N collision (the remainder of the decays producing three pions).

Figure 9(*a*) shows a comparison of the observed shower 'development' with that predicted by each of the above three models. (In this comparison, only the shapes and slopes are important†.)

A similar comparison of predictions from the Leeds models E, I and J (Hillas *et al* 1971) with observation is shown in figure 9(*b*).

In overall slope, the latest Sydney model appears to give the best fit to the observations; the Leeds model E, while not quite as steep as the observed, is nevertheless a reasonable fit.

Regarding the shape of the curves, the size of the errors in the observed points, and their scatter, makes little comment possible aside from the obvious discrepancy between the Sydney proton $E^{1/4}$ model and the observations for $\sec\theta \lesssim 1{\cdot}2$.

7. Primary energy spectrum

7.1. Description of the method and the results

Since the theoretical shower development models in general do not agree very well with the observed 'development', a primary energy has been assigned to each shower by first determining the equivalent vertical muon size $N'_{\mu 0}$ as defined by the shower development'

† In the absence of any independent energy determination, normalization is impossible, and therefore separations between model and observation on the 'lg N_μ' axis simply represent different energy assignments. Also, the slightly different N_μ ranges used in parts (*a*) and (*b*) of figure 9 were necessitated by the limited results from model calculation available.

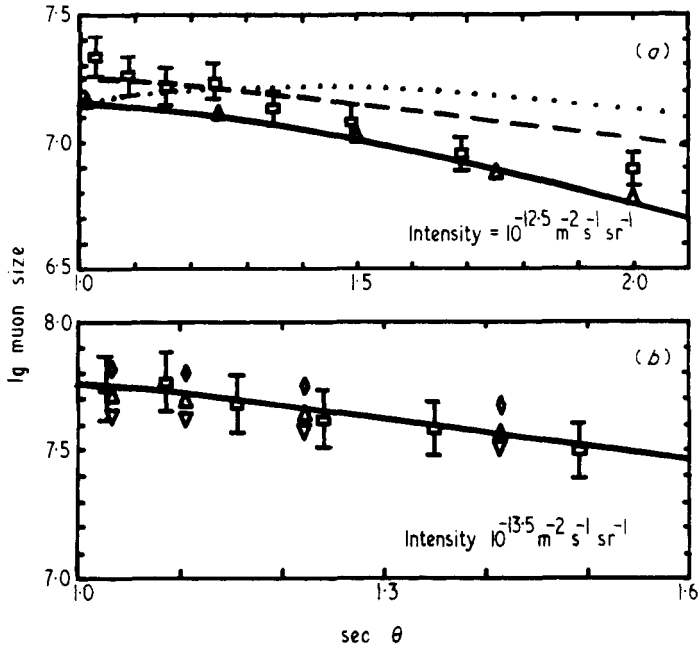

Figure 9. A comparison between theoretically predicted and observed shower development The theoretical predictions are not normalized to the observed curve (points $\frac{\Sigma}{\Sigma}$), so that only the shape and slope are significant. (*a*) Sydney development models; full curve with open triangle, latest model with $\chi = 1$; broken curve, copper $E^{1/4}$ Monte Carlo; dotted curve, proton $E^{1/4}$ Monte Carlo. (*b*) Leeds development models; ◇, model J; ▽, model I; △, model E.

curves of § 6.1. The muon size is then converted to primary energy using the predictions of the shower development model under consideration.

A maximum likelihood spectrum is fitted to the assigned energies in the same manner as for the muon size spectra (§ 5), except that a single zenith range, 0° to 56·8° ($=\sin^{-1}\sqrt{0{\cdot}7}$), has been used.

In the case in which energies were assigned according to the latest Sydney development model with $\chi = 1$, the differential spectrum fitted to 5347 showers in the range $10^{17{\cdot}25} < E < 10^{20{\cdot}25}$ eV is

$$J(E)\,dE = 10^{-29{\cdot}7\pm0{\cdot}01}\left(\frac{E}{10^{18}\,\text{eV}}\right)^{-2{\cdot}96\pm0{\cdot}02} dE\,\text{m}^{-2}\,\text{s}^{-1}\,\text{sr}^{-1}.$$

This spectrum, and the observed intensities in intervals of 0·25 in lg E_p, are shown in figure 10.

The error quoted here for the spectral index is the sum of the error contributed by the effective detecting area calculation and the error determined by the maximum likelihood fitting procedure (as the error required to reduce the likelihood by 0·5 from its maximum value, in other words, one standard deviation assuming a normal distribution). The error in the normalization constant is the sum of the error from poissonian variation in the total number of events and the error arising from the effective detecting area calculation. Errors arising from the energy assignment are swamped by the variation in energy

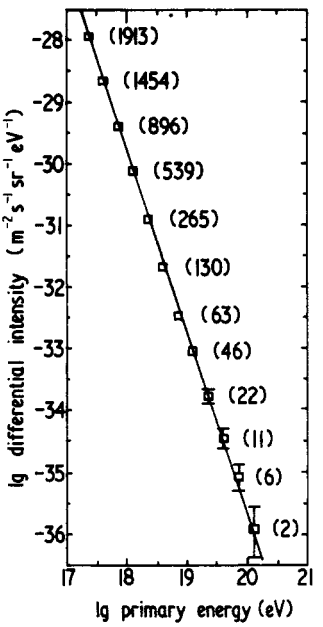

Figure 10. The differential energy spectrum calculated from SUGAR events 1 to 10065 using results from the latest Sydney shower development calculations to convert muon sizes to primary energies. The number of events contributing to each interval (of 0·25 in lg E) is indicated.

assignments by different models. The effect of errors arising from the shower size analysis is discussed in § 7.2.

The fitted spectrum was used to predict the number of events in each 0·25 interval in lg E_p, and a χ^2 test used to compare these predictions with the observed numbers. With nine degrees of freedom, the value of χ^2 was 43·8 (probability $< 0{\cdot}1\,\%$) which suggests that the fit to a straight line is not excellent; however, there is no *significant* evidence of any change in slope of the spectrum between 10^{19} and 10^{20} eV. In the determination of this value of χ^2, eleven cells were used corresponding to the points shown in figure 10 (the top two in energy being combined to bring the predicted frequency above five). Two degrees of freedom were subtracted for the maximum likelihood fit, one representing the total number of events (ie the normalization constant) and the other the slope. Since the maximum likelihood fit was made to the continuous distribution of events while the χ^2 test was applied to a grouping in cells, the number of degrees of freedom should be greater than nine, but in any case less than ten, and the probability of the result remains less than 0·1 %†. Several factors may have contributed to this improbability:

(i) the spectrum may in fact have small variations;

(ii) the assumption of isotropy at the highest energies may be incorrect, leading to miscalculation of the detection solid angle.

Primary energy spectra have been calculated from the SUGAR data using muon-size to primary-energy conversions derived from all the Sydney and Leeds shower

† The maximum likelihood method involved the solution of the conditions for maximum; the actual likelihood was not determined since its normalization required integration over the entire (k, γ) space.

development models for which they are available. The results are shown in table 1, in the form

$$J(>E) = k\left(\frac{E}{10^{18}\,\mathrm{eV}}\right)^{-\gamma} \mathrm{m}^{-2}\,\mathrm{s}^{-1}\,\mathrm{sr}^{-1}.$$

The integral spectral slopes range from $-1{\cdot}81$ to $-2{\cdot}12$ and the intensity at 10^{19} eV ranges from $10^{-14{\cdot}66}$ to $10^{-12{\cdot}72}\,\mathrm{m}^{-2}\,\mathrm{s}^{-1}\,\mathrm{sr}^{-1}$. Restricting the conversions to those derived from the Sydney (copper, $E^{1/4}$) Monte Carlo model and the latest model with $\chi = 1$, and from the preferred Leeds models, E, I and J, the range of slopes becomes $-1{\cdot}97$ to $-2{\cdot}12$ and of intensities at 10^{19} eV, $10^{-14{\cdot}66}$ to $10^{-13{\cdot}25}\,\mathrm{m}^{-2}\,\mathrm{s}^{-1}\,\mathrm{sr}^{-1}$. By comparison, the latest estimate (Edge *et al* 1973) of the slope of the Haverah Park integral energy spectrum is $-2{\cdot}17 \pm 0{\cdot}03$.

Except for the (copper, $E^{1/4}$) model, all models estimate the highest energy showers as being above 10^{20} eV.

Table 1.

Conversion model	γ	lg k	Fitted in range of lg E	χ_n^2	n	0·1 % value of χ_n^2
Sydney						
proton $E^{1/4}$	$1{\cdot}97 \pm 0{\cdot}02$	$-12{\cdot}19 \pm 0{\cdot}01$	17·25 to 20·25	37·5	8	26·1
proton in E	$1{\cdot}81 \pm 0{\cdot}02$	$-11{\cdot}68 \pm 0{\cdot}01$	17·50 to 20·75	34·0	9	27·9
copper $E^{1/4}$	$1{\cdot}98 \pm 0{\cdot}03$	$-12{\cdot}67 \pm 0{\cdot}01$	17·25 to 20·00	26·7	7	24·3
copper in E	$1{\cdot}87 \pm 0{\cdot}02$	$-12{\cdot}41 \pm 0{\cdot}01$	17·25 to 20·25	30·8	8	26·1
latest $\chi = 1$	$1{\cdot}96 \pm 0{\cdot}02$	$-12{\cdot}03 \pm 0{\cdot}01$	17·25 to 20·25	43·8	9	27·9
Hillas						
A	$2{\cdot}07 \pm 0{\cdot}03$	$-11{\cdot}63 \pm 0{\cdot}01$	17·75 to 20·50	27·6	7	24·3
D	$1{\cdot}99 \pm 0{\cdot}02$	$-10{\cdot}73 \pm 0{\cdot}01$	18·00 to 21·00	34·3	8	26·1
E	$2{\cdot}07 \pm 0{\cdot}02$	$-11{\cdot}42 \pm 0{\cdot}01$	17·75 to 20·50	29·6	7	24·3
F	$2{\cdot}08 \pm 0{\cdot}02$	$-11{\cdot}83 \pm 0{\cdot}01$	17·75 to 20·25	32·2	8	26·1
H	$2{\cdot}12 \pm 0{\cdot}02$	$-11{\cdot}73 \pm 0{\cdot}01$	17·50 to 20·25	38·3	8	26·1
I	$2{\cdot}01 \pm 0{\cdot}02$	$-11{\cdot}24 \pm 0{\cdot}01$	17·75 to 20·50	37·7	8	26·1
J	$2{\cdot}12 \pm 0{\cdot}03$	$-11{\cdot}59 \pm 0{\cdot}01$	17·75 to 20·25	27·9	7	24·3
K	$2{\cdot}02 \pm 0{\cdot}02$	$-10{\cdot}92 \pm 0{\cdot}01$	18·00 to 20·75	29·6	8	26·1

7.2. Testing the analysis by simulation

To detect biases in the analysis, particularly from the spread in muon sizes and energies fitted to showers originating from primary particles with the same energy, a set of showers was simulated as described in § 3.3 with an energy spectrum

$$J(E)\,\mathrm{d}E = 10^{-30{\cdot}30}\left(\frac{E}{10^{18}\,\mathrm{eV}}\right)^{-3{\cdot}00} \mathrm{d}E\,\mathrm{m}^{-2}\,\mathrm{s}^{-1}\,\mathrm{sr}^{-1}.$$

These showers were then subjected to the normal analysis for arrival direction and muon size, and a spectrum was fitted to the results:

$$J(E)\,\mathrm{d}E = 10^{-30{\cdot}35 \pm 0{\cdot}06}\left(\frac{E}{10^{18}\,\mathrm{eV}}\right)^{-3{\cdot}04 \pm 0{\cdot}08} \mathrm{d}E\,\mathrm{m}^{-2}\,\mathrm{s}^{-1}\,\mathrm{sr}^{-1}.$$

The input spectrum and the fitted spectrum are compared in figure 11. Both the spectral

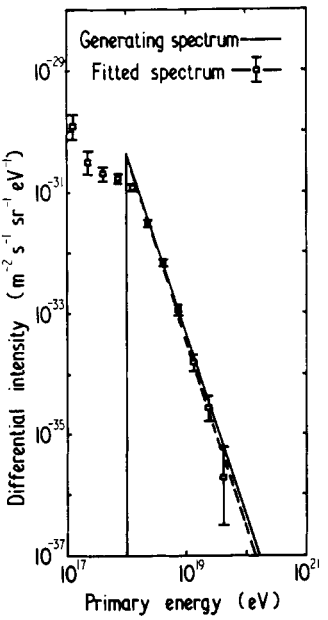

Figure 11. A comparison of the energy spectrum fitted to a set of simulated showers with the spectrum from which they were generated. Individual intensities in intervals of 0·25 in lg E are also shown.

index and the intensities for $E > 10^{18}$ eV were reproduced within the errors. Below this energy (slightly to $E \sim 10^{18\cdot25}$ eV and then significantly for $E < 10^{18\cdot25}$) there is a fall-off in intensity due to scattering of the fitted energies about the simulated energies near to the cut-off in the simulated energies. In other words, just above this cut-off there is a reduction in intensity due to scattering downward in energy, with no compensating increase in intensity due to scattering upward from below the cut-off.

It was noted before (§ 3.3) that an average reduction in lg E_p of 0·15 occurs in the analysis. The preservation of the simulated spectrum through the analytical system shows that this, and the tendency for those showers whose energy is increased to have a more significant effect, roughly balance out and so do not alter the overall slope and intensity of the spectrum. However, small-scale variations would tend to be smoothed out.

7.3. Composite energy spectrum

The spectra from § 7.1 are compared with the results from other experiments in figure 12. These results are from (1) Volcano Ranch (Clark *et al* 1961 and Linsley 1963), (2) Sydney 64S array (Jauncey 1965), (3) Moscow (Khristiansen *et al* 1965), (4) Mount Chacaltaya (La Pointe *et al* 1968), (5) Haverah Park (Edge *et al* 1973) and (6) Yakutsk (Egorov *et al* 1971).

It is interesting to compare the Haverah Park spectrum derived using the Leeds model E shower development calculations to assign the shower energies, with the Sydney spectrum also derived using the same model to assign shower energies. As a background to this, the actual shower observations involved can also be compared. Dixon *et al* (1973) have measured the density of muons of momentum greater than

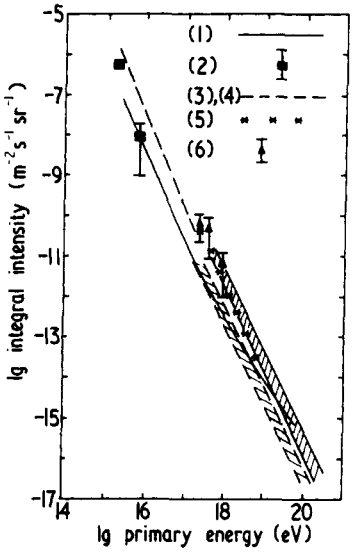

Figure 12. A composite integral energy spectrum showing results from other experiments ((1) to (6)) and from the SUGAR data using muon-size to primary-energy conversions based on Sydney (hatched horizontally) and Leeds (hatched vertically) shower development calculations.

1 GeV/c at a distance of 300 m from the shower core for a near-vertical shower of energy 2×10^{17} eV as assigned by the Haverah Park array via the Leeds model E results, as 0·46 m^{-2}. For a shower of the same energy as assigned by the SUGAR array via the Leeds model E results, the density of muons of energy greater than 0·75 GeV at a core distance of 300 m is 0·47 m^{-2} according to the standard SUGAR structure function. Because of the flatness of the muon energy spectrum for muons of momentum about 1 GeV/c in a shower of this size, the difference in the thresholds may be neglected. Thus the observations are in reasonable agreement.

A comparison between the two (differential) spectra calculated via model E is shown in figure 13. The individual intensities plotted are in slightly better agreement than the fitted spectra. The Haverah Park intensities were calculated from table 5 of Edge *et al* (1973) using $\rho(600)=\rho(500)/1{\cdot}8$ and $E=3{\cdot}87\times10^{17}\,\rho(500)^{1{\cdot}018}$ (Andrews *et al* 1971).

Specifically these spectra are:

$$J(>E)=(4{\cdot}3\pm0{\cdot}1)\times10^{-10}\left(\frac{E}{10^{17}\,\mathrm{eV}}\right)^{-2{\cdot}18\pm0{\cdot}02}\ \mathrm{m^{-2}\,s^{-1}\,sr^{-1}}$$

or

$$J(E)\,\mathrm{d}E=10^{-29{\cdot}21\pm0{\cdot}01}\left(\frac{E}{10^{18}\,\mathrm{eV}}\right)^{-3{\cdot}18\pm0{\cdot}02}\mathrm{d}E\,\mathrm{m^{-2}\,s^{-1}\,sr^{-1}}\qquad\text{(Haverah Park)}$$

and

$$J(>E)=10^{-11{\cdot}42\pm0{\cdot}01}\left(\frac{E}{10^{18}\,\mathrm{eV}}\right)^{-2{\cdot}07\pm0{\cdot}02}\ \mathrm{m^{-2}\,s^{-1}\,sr^{-1}}$$

or

$$J(E)\,\mathrm{d}E=10^{-29{\cdot}10\pm0{\cdot}01}\left(\frac{E}{10^{18}\,\mathrm{eV}}\right)^{-3{\cdot}07\pm0{\cdot}02}\mathrm{d}E\,\mathrm{m^{-2}\,s^{-1}\,sr^{-1}}\qquad\text{(Sydney).}$$

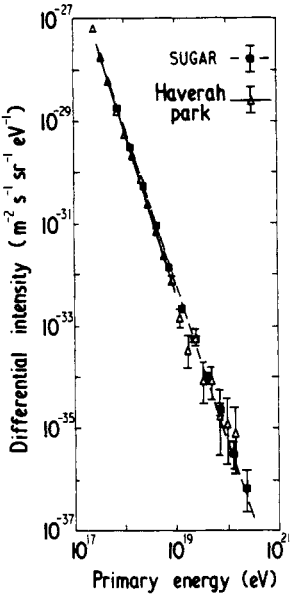

Figure 13. A comparison between energy spectra derived from the Haverah Park (Edge *et al* 1973) and SUGAR experiments, in both cases by assigning energies according to the Leeds shower development model E.

The difference between the intensities at high energies can be seen in the numbers of such showers actually detected: the Haverah Park array, with an exposure of approximately 15 km^2 yr, has observed 28 showers above 10^{19} eV and 2 above 10^{20} eV (Edge *et al* 1973), while the SUGAR array with 175 km^2 yr has observed 157 showers above 10^{19} eV and 6 above 10^{20} eV (by the Leeds model E energy conversion). This comparison takes no account of differences in acceptance solid angle between the arrays, which would be slight. The solid angle for the Haverah Park array would tend to be slightly less than that for the SUGAR array since Haverah Park detects the electromagnetic component as well as the muon component, and hence the effective shower attenuation length should be shorter (although the measured value, 760 g cm^{-2} according to Edge *et al* 1973, is virtually identical).

A recent event (not included in the spectral analysis) detected by the SUGAR array is a candidate for the highest-energy cosmic ray yet recorded. The standard SUGAR analysis has assigned the shower, whose zenith angle is 42°, a primary energy of $2{\cdot}1 \times 10^{20}$ eV, using the latest Sydney shower development model, with $\chi = 1$. The Leeds model E gives $3{\cdot}3 \times 10^{20}$ eV. Eight stations were involved in the event (ie sixteen scintillators), of which a map, in a plane perpendicular to the shower axis, is shown in figure 14. The numbers indicate the recorded muon density in particles/m^2.

There are some problems with the analysis of such a shower. The north tank of station 2 recorded a saturated response (density >800 m^{-2}) and the standard analysis placed the shower core on this tank. However, in a shower as large as this, such densities may occur at distances up to several hundred metres from the core. Further, for very large responses, afterpulsing in the photomultiplier tube can falsify the logarithmic pulse-height to time conversion used by lengthening the pulse, leading to an over-estimate of the muon density. The shower was therefore re-analysed assigning lower

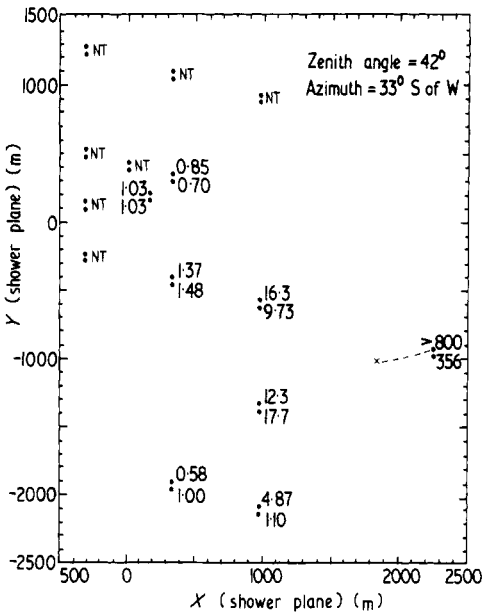

Figure 14. A map of event 12420, in a plane perpendicular to the shower axis, showing the muon density (m^{-2}) at each scintillator of each station. NT indicates not triggered, that is, with a density less than 0·5 muons m^{-2} at one or both tanks. Stations which were inoperative at the time of the event (either through 'dead' time from a previous event or from faulty apparatus) are not shown. In particular, station 1 to the north of station 2 was in 'dead' time, while station 3 to the south was recording faulty timing patterns. The locus of core positions down to that given by densities of (100, 100) m^{-2} at station 2 is indicated by the dashed line.

densities to the station 2 responses and allowing the core to move from the saturated tank. Since the probability of recording a saturated response from an actual density less than 100 m^{-2} is negligible, this value of density (in *both* tanks of station 2) was used, and yielded a *minimum* primary energy of $7{\cdot}9 \times 10^{19}$ eV ($1{\cdot}3 \times 10^{20}$ eV by Leeds model E). The most probable estimate would appear to be in the vicinity of 10^{20} eV ($1{\cdot}6 \times 10^{20}$ eV by Leeds model E).

8. Conclusions

In the absence of an accepted model for the development of air showers initiated by cosmic rays of energy in the region 10^{17} to 10^{21} eV, no final primary energy spectrum can be presented. However, it appears likely that the spectrum extends beyond 10^{20} eV with no significant features, and with an integral spectral index between 1·97 and 2·12. The preferred integral spectrum, fitted to showers whose energy has been assigned by the latest Sydney shower development model with $\chi = 1$, is:

$$J(>E) = 10^{-12{\cdot}03 \pm 0{\cdot}01}\left(\frac{E}{10^{18}\,\text{eV}}\right)^{-1{\cdot}96 \pm 0{\cdot}02} \text{m}^{-2}\text{s}^{-1}\text{sr}^{-1}$$

for energies in the range $10^{17{\cdot}25} \leqslant E \leqslant 10^{20{\cdot}25}$ eV. If copper primaries rather than proton primaries were assumed, the energies would be reduced by a factor of about 1·5

but the slope of the spectrum would remain unchanged. The upper limit of the spectrum would be 10^{20} eV. (This spectrum differs slightly from that quoted at the Denver Conference on cosmic rays (Bell *et al* 1973) in that it involves a complete recalculation of the spectrum using the latest Sydney shower development calculations to convert muon sizes to energies. The spectrum presented at Denver was obtained simply by adjusting the spectrum derived using the older (proton, $E^{1/4}$) Sydney calculations which give energies very close to the latest calculations.)

Acknowledgments

We are indebted to the Australian Research Grants Committee, The Science Foundation for Physics within the University of Sydney and the United States Air Force for grants enabling this project to be initiated and continued over the past seven years. We are also extremely grateful to Professor H Messel for the provision of the very excellent research facilities within the School of Physics, University of Sydney.

References

Andrews D *et al* 1971 *Proc. 12th Int. Conf. on Cosmic Rays, Hobart* vol 3 (Hobart: University of Tasmania) pp 995–1000

Bell C J *et al* 1973 *Proc. 13th Int. Conf. on Cosmic Rays, Denver* vol 4 (Denver: University of Denver) pp 2519–24

Bennett S and Greisen K 1961 *Phys. Rev.* **124** 1982

Brownlee R G *et al* 1970 *Acta Phys. Acad. Sci. Hung.* **29** *Suppl.* 3 651–5

Clark G W *et al* 1961 *Phys. Rev.* **122** 637

Dixon H E *et al* 1973 *Proc. 13th Int. Conf. on Cosmic Rays, Denver* vol 4 (Denver: University of Denver) pp 2556–61

Edge D M *et al* 1973 *J. Phys.* A: *Math., Nucl. Gen* **6** 1612–34

Egorov T A *et al* 1971 *Proc. 12th Int. Conf. on Cosmic Rays, Hobart* vol. 6 (Hobart: University of Tasmania) pp 2059–73

Fisher A J 1970 *PhD Thesis* University of Sydney

Goorevich L 1971 *Proc. 12th Int. Conf. on Cosmic Rays, Hobart* vol 3 (Hobart: University of Tasmania) pp 983–8

Goorevich L and Peak L S 1973 *Proc. 13th Int. Conf. on Cosmic Rays, Denver* vol 4 (Denver: University of Denver) pp. 2617–24

Jauncey D L 1965 *PhD Thesis* University of Sydney

Khristiansen G B *et al* 1965 *Proc. 9th Int. Conf. on Cosmic Rays, London* vol 2 (London: The Institute of Physics and The Physical Society) p 799

La Pointe M *et al* 1968 *Can. J. Phys.* **46** S68

Linsley J 1963 *Proc. 8th Int. Conf. on Cosmic Rays, Jaipur* vol 4 (Bombay: TIFR) pp 77–99

McCusker C B A *et al* 1970 *Acta Phys. Acad. Sci. Hung.* **29** *Suppl.* 3 527–31